ELSEVIER

PII: S0032-3861(97)00111-0

*Polymer* Vol. 38 No. 22, pp. 5521–5538, 1997
© 1997 Elsevier Science Ltd
Printed in Great Britain. All rights reserved
0032-3861/97/$17.00+0.00

# Time resolved simultaneous small- and wide-angle X-ray scattering during polyethylene deformation: 1. Cold drawing of ethylene-$\alpha$-olefin copolymers

**Michael F. Butler and Athene M. Donald***
*Department of Physics, Cavendish Laboratory, University of Cambridge, Madingley Road, Cambridge, CB3 0HE, UK*

**and Anthony J. Ryan**
*Materials Science Centre, UMIST, Grosvenor Street, Manchester, M1 7HS and CCLRC Daresbury Laboratory, Daresbury, Warrington, Cheshire, WA4 4AD, UK*
*(Received 19 September 1996; revised 29 November 1996)*

The cold drawing behaviour of a range of polyethylene copolymers was investigated using the technique of simultaneous small- and wide-angle X-ray scattering (SAXS and WAXS, respectively) during deformation. The influence of branch amount, branch length and lamellar population were studied. Branch length was found to be unimportant. Increasing branch content lowered the percentage crystallinity which resulted in an increase in the importance of interlamellar deformation mechanisms. Double yield points were observed in some samples. Molecular and lamellar deformation was totally reversible up to the first yield point, and was apportioned to the activation of fine chain slip. After the second yield point, for which coarse chain slip leading to lamellar fragmentation was held responsible, deformation was irreversible. © 1997 Elsevier Science Ltd.

**(Keywords: X-ray scattering; branched polyethylene; cold drawing)**

## INTRODUCTION

The inclusion of short chain branches by copolymerizing ethylene with an $\alpha$-olefin markedly affects the mechanical behaviour of polyethylene (PE)[1,2]. Only a few branches per 1000 C atoms result in a vast improvement in creep resistance[3,4]. Environmental stress cracking resistance (ESCR) is also improved via the influence of side chain branching on the microstructure[5,6].

When attempting to understand the deformation of PE copolymers several factors must be evaluated. As well as molecular weight, polydispersity and percentage crystallinity, the chemical nature of the comonomer, the quantity and distribution of the branches, and their inclusion into the crystalline lamellae must be considered. Whether the branches enter the lamellae on an equilibrium basis is important; methyl branches do[7] and methyl branched PE is more similar to linear PE than copolymer containing longer branches[1]. Longer branches are excluded into the interfacial and interlamellar regions[8], although in fast-cooled samples there may be some non-equilibrium entry[9].

The exclusion of branched material from lamellae results in a decrease of long spacing and lamellar thickness with increasing number of branches. Assuming that a tie molecule forms when the end to end distance of a molecule in the melt is equal to or greater than the distance between adjoining lamellae it follows that a reduced long spacing results in a higher tie molecule density[4]. Increasing tie molecule density increases toughness[5,10]. Branches are most effective in improving the mechanical properties when they are placed on longer molecules, i.e. those most likely to act as tie molecules[11]. It is proposed that the formation of a continuous network by the tie molecules and the large amount of disentanglement that is required to achieve large plastic deformations is responsible for the large improvement in creep resistance[1,11–13].

The presence of a branch on a tie molecule increases the resistance to disentanglement[3,11]. De Gennes has shown that the presence of branches significantly decreases chain mobility[14]. The resistance will increase with amount of branches, which explains the increase in strain hardening as branch amount increases[1,2]. Some workers have found evidence for the importance of branch length[1,2,6], since shorter ethyl branches are expected to offer less disentanglement resistance than longer butyl, iso-butyl or hexyl branches, although branch length is of lesser importance than branch amount[11].

Branch distribution also affects the tie molecule

* To whom correspondence should be addressed

density. Two samples may have similar percentage crystallinities, but different lamellar and interlamellar thicknesses depending on both the side-chain spacing on the main chains and the branch distribution with respect to the molecular weight distribution. The reduction in percentage crystallinity with increasing branch content is responsible for a decrease in yield stress[1,2].

In this paper the effects of branch amount, distribution and length, as well as lamellar population, on cold drawing, are reported. The small-angle X-ray scattering (SAXS) and wide-angle X-ray scattering (WAXS) were measured simultaneously, as described previously[15]. In addition, the load–extension curve was simultaneously measured, enabling precise relation of the microscopic and macroscopic deformation.

## EXPERIMENTAL

### *Materials and sample preparation*

A range of branched polyethylenes (MDPE and LLDPE), containing ethyl, butyl and iso-butyl branches, supplied by BP Chemicals Ltd. (Sunbury, UK) were used in this study. $M_w$ values lay between 120 000 and 206 000. Sample information is summarized in *Table 1*.

**Table 1** Sample information

| Sample | $M_w$ (1000) | $M_w/M_n$ | Branch type | Branch amount SCB/1000C |
|---|---|---|---|---|
| HDPE | | | | |
| B | 131.0 | 6.3 | N/A | N/A |
| MDPE | | | | |
| C | 206.0 | 8.6 | Butyl | 6.2 |
| LLDPE | | | | |
| G | 152.1 | 5.2 | Ethyl | 23.71 |
| H | 126.0 | 4.2 | Iso-butyl | 21.0 |
| I | 110.0 | 3.0 | Butyl | ~20 |
| J | 103.0 | 2.8 | Butyl | ~20 |

Plaques, 0.9 mm thick, were formed by compression moulding the molten PE using the method described previously[15]. Specially shaped samples for tensile testing were punched from these plaques. They were 50 mm long and 20 mm wide, with two semi-circular cut-outs of radius 8 mm to ensure that yielding always occurred in the beam.

Some samples were annealed in order to change the percentage crystallinity lamellar thickness and lamellar population. Samples C, G and H were annealed under vacuum at 114°C for 22 h and I and J were annealed for 17 h at 114°C. They were cooled slowly (initial cooling rate 0.5°C $min^{-1}$) to room temperature. The annealed samples are denoted by SC, and the unannealed ones by U, to match previous notation.

### *Differential scanning calorimetry*

Differential scanning calorimetry (d.s.c) was used to obtain the percentage crystallinity of the samples and information on the lamellar populations and thicknesses. Measurements were taken on a Perkin Elmer DSC7 equipped with an Intracooler II and calibrated with indium and zinc. The lamellar thickness, $L_c$, was estimated by rearranging the equation for the melting point, $T_m$,

$$L_c = \frac{2\sigma_e}{\Delta h} \frac{T_{m0}}{T_{m0} - T_m} \quad (1)$$

Using the value of $(93 \pm 8) \times 10^{-7}$ J $cm^{-2}$ for the fold surface energy $\sigma_e$[16], employing 280 J $cm^{-3}$ for the heat of fusion of crystal, $\Delta h$[16], and taking the equilibrium melting temperature, $T_{m0}$, to be equal to 145.8°C[16], lamellar thicknesses were estimated.

The percentage crystallinity was calculated from the specific heat of fusion by taking the specific heat of fusion of perfectly crystalline PE to be 293 J $g^{-1}$ [17]. An estimate

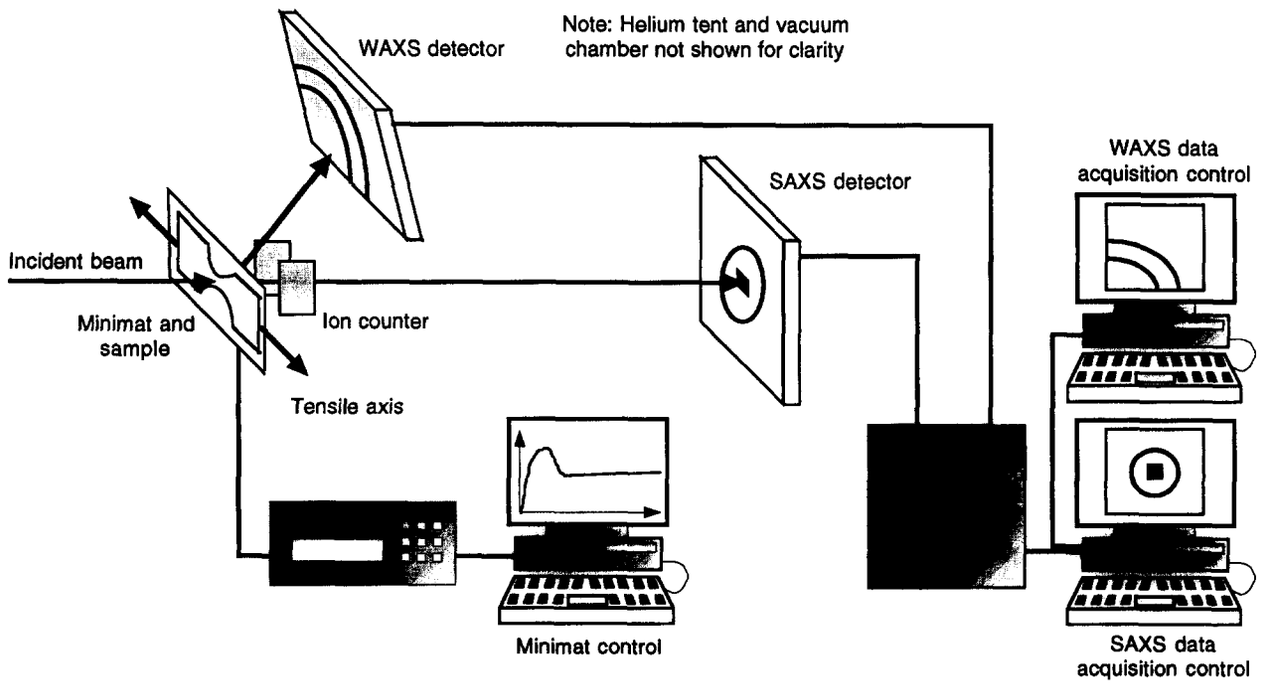


**Figure 1** Schematic diagram of the experimental setup

for the lamellar thickness from the SAXS long spacing, $d$, was made using the two phase model from the lamellar thickness, $L_c$, and the percentage crystallinity, $\chi$, for comparison with d.s.c. results.

$$L_c = \chi d \tag{2}$$

*Simultaneous SAXS/WAXS measurement during* in situ *deformation*

X-ray scattering experiments were performed on beamlines 2.1[18] and 16.1[19,20], at the Synchrotron Radiation Source (SRS) at Daresbury in the UK, with the set-up described previously (shown in *Figure 1*[15,21]). Two-dimensional SAXS and WAXS patterns were obtained simultaneously using gas filled multiwire area detectors from the highly deformed necked region of the sample. The size of the beam on the sample was approximately 0.5 mm × 0.5 mm. At yield, when deformation was highly localized, the beam size had approximately the same dimensions as the deformed region. As drawing progressed, however, the beam size became substantially smaller than the size of the deformed region of the sample. It was possible, therefore, that in the yielding stages of deformation, the SAXS and WAXS patterns were averaged over a spread of extension ratios. This effect will, however, decrease as the sample neck develops. In order to investigate the localization of the deformation in the neck the deformation of some samples were investigated in the region adjacent to the neck. Samples were drawn at an extension rate of 5.0 mm $min^{-1}$.

Additionally, image plates were used to collect the full wide-angle diffraction pattern for some samples drawn at 1 mm $min^{-1}$. The sample was exposed to the X-ray beam at selected points on the load–extension curve. Samples C and H which had just yielded were allowed to physically relax without load and examined approximately 1 h later.

The Lorentz correction, which corresponds to multiplying the intensity by $q^2$, where **q** is the scattering vector, was applied to all the SAXS data. The scattering vector is taken to be

$$|\mathbf{q}| = q = \frac{2\pi}{d} = \frac{4\pi}{\lambda} \sin\theta \tag{3}$$

**Table 2** Information from d.s.c.

| Sample | Lamellar thickness(es) (nm) | Percentage crystallinity | Neck percentage crystallinity |
|---|---|---|---|
| B U | 32.00 ± 2.80 | 74.9 ± 0.3 | 58.7 ± 0.5 |
| C U | 13.85 ± 1.19 | 52.3 ± 0.2 | 51.0 ± 0.3 |
| C SC | (1) 10.32 ± 0.89 | 55.7 ± 0.9 | 52.8 ± 0.2 |
| | (2) 17.91 ± 1.54 | | |
| G U | 12.27 ± 1.06 | 37.5 ± 0.4 | 38.1 ± 0.2 |
| G SC | (1) 6.10 ± 0.52 | 39.5 ± 1.0 | 40.0 ± 0.3 |
| | (2) 13.33 ± 11.5 | | |
| H U | 14.37 ± 1.24 | 39.0 ± 0.4 | 38.9 ± 0.4 |
| H SC | (1) 5.80 ± 0.50 | 42.2 ± 0.4 | 40.2 ± 0.4 |
| | (2) 10.39 ± 0.89 | | |
| | (3) 14.79 ± 1.27 | | |
| I U | 13.74 ± 1.18 | 37.9 ± 0.7 | 38.0 ± 0.4 |
| I SC | (1) 5.25 ± 0.45 | 39.4 ± 0.2 | 39.7 ± 0.9 |
| | (2) 9.38 ± 0.81 | | |
| | (3) 14.20 ± 1.22 | | |
| J U | 12.41 ± 1.07 | 34.9 ± 0.9 | 39.1 ± 0.5 |
| J SC | (1) 5.62 ± 0.48 | 37.0 ± 0.8 | 36.9 ± 2.2 |
| | (2) 10.02 ± 0.86 | | |
| | (3) 12.82 ± 1.10 | | |

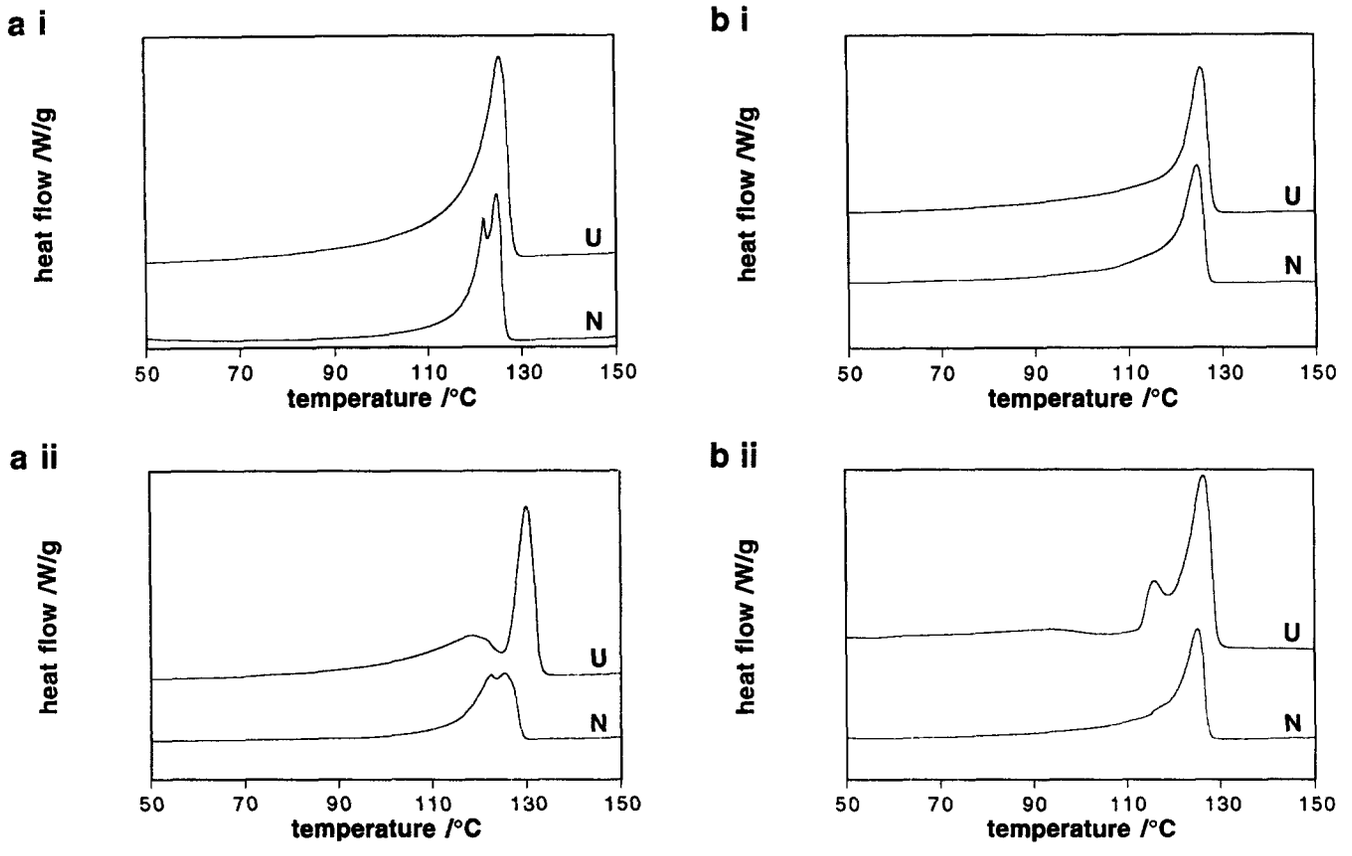


**Figure 2** D.s.c. traces from undeformed (U) and necked (N) material from (a) MDPE sample I and (b) LLDPE sample C. In both cases (i) is for the untreated sample and (ii) is for the annealed sample

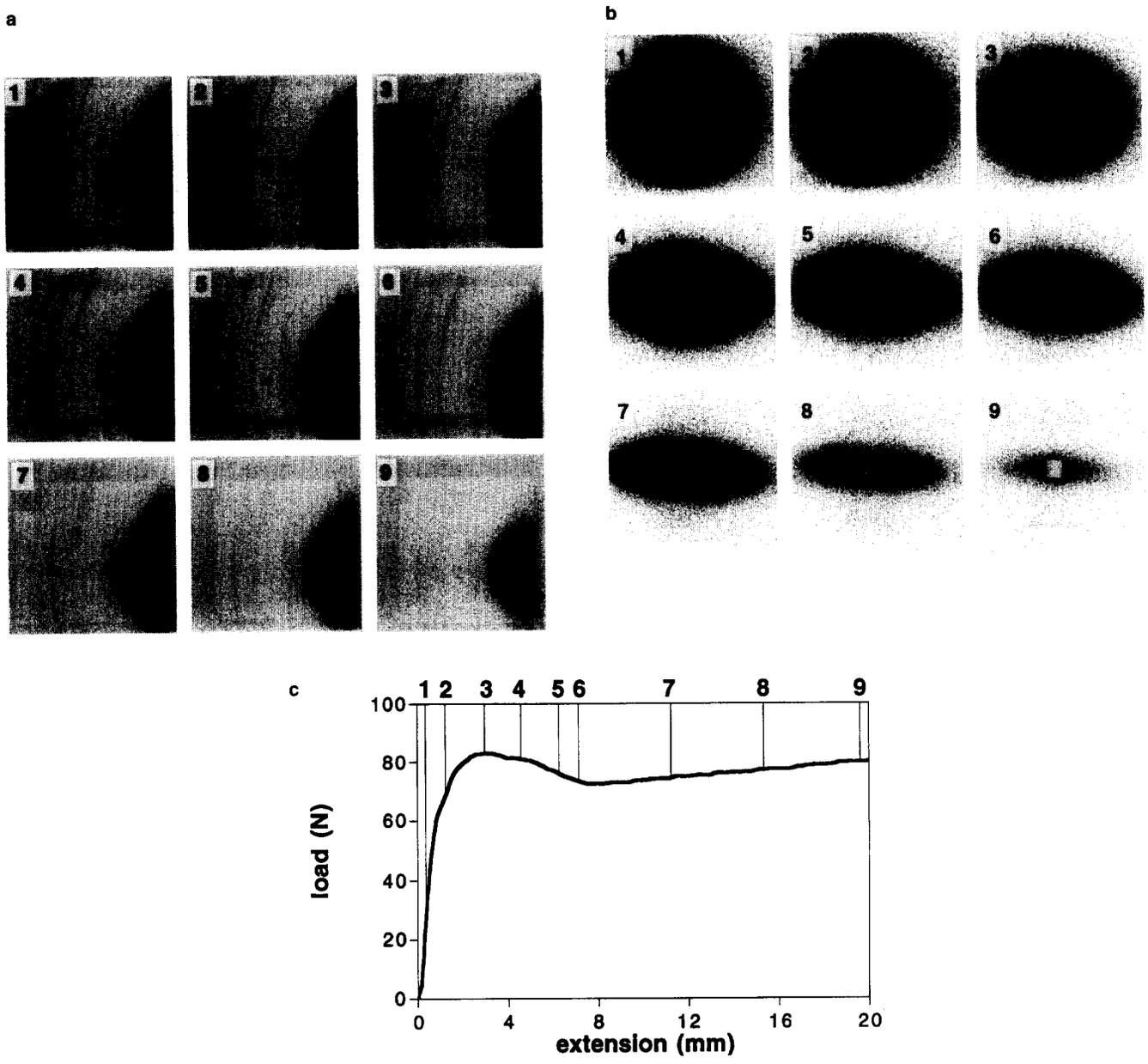


**Figure 3** Series of simultaneously obtained (a) equatorial WAXS and (b) SAXS patterns, along with (c) the load–extension curve, for unannealed G. The points at which the X-ray scattering patterns were obtained are marked on the load–extension curve. In (a) and (b) the tensile axis is vertical

where $d$ is the long spacing, $\lambda$ the X-ray wavelength and $\theta$ the scattering angle. The Lorentz correction is necessary in a randomly oriented sample to correct for the different probabilities of planes being in the reflection condition[22]. In applying this correction the assumption is made that the morphology is locally lamellar but globally isotropic[23], i.e. that the lamellae are randomly oriented throughout the whole sample, which is correct for undeformed PE but less so when the structure has become fibrillar.

## RESULTS

### *D.s.c.*

All of the untreated samples had one melting point. Annealing caused extra melting endotherms to appear at lower temperatures. Samples G, H, I and J gained two extra endotherms and sample C gained one extra endotherm. No lamellar thickening occurred for the LLDPE grades, but there was an increase in percentage crystallinity upon annealing of between 2 and 4%. Lamellar thickening and an increase in percentage crystallinity occurred for the MDPE grade, C. The percentage crystallinities and lamellar thicknesses obtained from d.s.c. are shown in *Table 2*. D.s.c. traces are shown for unannealed and annealed I, from both undeformed and necked material, to illustrate the LLDPEs, and from C, to illustrate the MDPE, in *Figures 2a* and *b* respectively.

In the drawn material the lamellar population and percentage crystallinity changed. In untreated C the lamellar population became bimodal, with the appearance of a new lower temperature melting endotherm, and the percentage crystallinity decreased. In annealed C the lamellar population remained bimodal, although the melting peaks shifted to lower temperatures, and the percentage crystallinity decreased.

The untreated LLDPEs retained their unimodal lamellar thickness distribution on drawing. In G and J

the percentage crystallinity increased whereas in H and I it was unchanged. The percentage crystallinity also remained unchanged for annealed H, I and J, but decreased for annealed G. The lower temperature melting endotherms were almost completely lost on drawing for all of the annealed LLDPEs and the lamellar thickness distribution became unimodal.

*Tensile properties*

All of the branched PE grades were ductile. Double yield points were observed in untreated C, G and J. The yielding region was more diffuse than for the linear HDPE grade B of similar molecular weight. Annealed samples had sharper yield points. The yield extension increased with increased branch amount. All of the untreated LLDPEs yielded at approximately the same extension. Annealed G and H yielded at a higher extension than the untreated samples, whereas the opposite was found for the butyl branched LLDPE samples, I and J.

The yielding and strain-softening region of the load–extension curve occurred over an extension of several millimetres (compared to the beam size of 0.5 mm × 0.5 mm). Therefore the concern over whether the SAXS and WAXS patterns were averaged over a range of material deformed to different extents is shown to be relevant only at the very point of yielding, where some of the beam may have overlapped the forming neck and the adjacent virtually undeformed material. This situation diminished in importance very rapidly after the yield point, as the dimensions of the neck exceeded that of the beam.

*WAXS*

All of the grades behaved in a qualitatively similar manner which has been described in more detail previously[15]. A series of simultaneously obtained equatorial WAXS patterns and SAXS patterns are shown in *Figure 3* with the load–extension curve for unannealed G. *Figure 4* shows a series of meridional WAXS patterns and load–extension curve, collected from a separate sample (the SAXS patterns are not shown). The SAXS results will be described later.

In *Figure 5* the full WAXS patterns are shown for annealed C for (a) the undeformed sample, (b) before the yield point during elastic deformation, (c) at the yield point, (d) during strain softening and (e) in the plateau region when the sample had necked. *Figure 5f* shows the WAXS pattern of a sample taken to the yield point (until the WAXS pattern was like *Figure 5c*) and then relaxed for 1 h after release from load. The simultaneously obtained load–extension curve is shown in *Figure 5g*. A well defined fibre pattern can be seen once the sample was well into the load–extension plateau (*Figure 5e*).

The evolution of the WAXS intensities for all of the LLDPE samples is shown in *Figure 6*. The martensitic transformation occurred in all samples at the yield point (defined as the maximum in the load–extension curve), shown in *Figure 7* for all samples. The onset of the martensitic transformation was identified by the appearance of the monoclinic (0 0 1) reflection in the meridional WAXS patterns, shown in *Figure 4*, and the much weaker monoclinic ($\bar{2}$ 0 1) reflection in the equatorial WAXS patterns shown in *Figure 3*. The full WAXS pattern shown in *Figure 5* is useful since it shows that the monoclinic (0 0 1) reflection is a wide arc, although centred on the meridian nevertheless. The transformation was active during the yielding and strain-softening region, shown by the increase in intensity of the monoclinic ($\bar{2}$ 0 1) reflection in this region only. After strain softening was complete the monoclinic ($\bar{2}$ 0 1) intensity remained constant, as can be seen in *Figure 8*. *Figure 9* shows that the strain range over which the martensitic transformation occurred (defined as the strain range over which the monoclinic ($\bar{2}$ 0 1) reflection was increasing in intensity) was directly related to the percentage crystallinity.

*Orientation*

In all of the samples there was no discernible orientation until the (first) yield point was reached. From *Figure 6* it can be seen that changes in WAXS peak intensity occur over quite a small range of extension. *Figure 8* shows that the changes occurred during yield and strain softening, using the orthorhombic (1 1 0) and monoclinic ($\bar{2}$ 0 1) reflections for illustration. It was found, as previously[15], that the decrease in orthorhombic

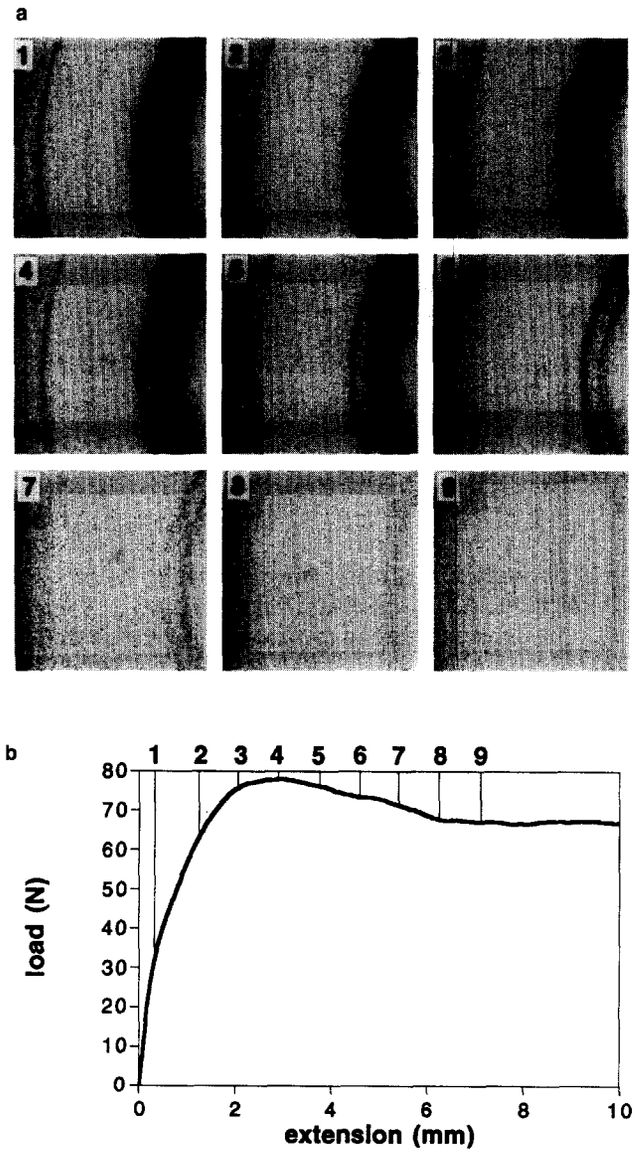


**Figure 4** Series of (a) meridional WAXS patterns and (b) simultaneously obtained load–extension curve for unannealed G. The SAXS patterns are not shown, since they are identical to those in *Figure 3*. In (a) the tensile axis is horizontal

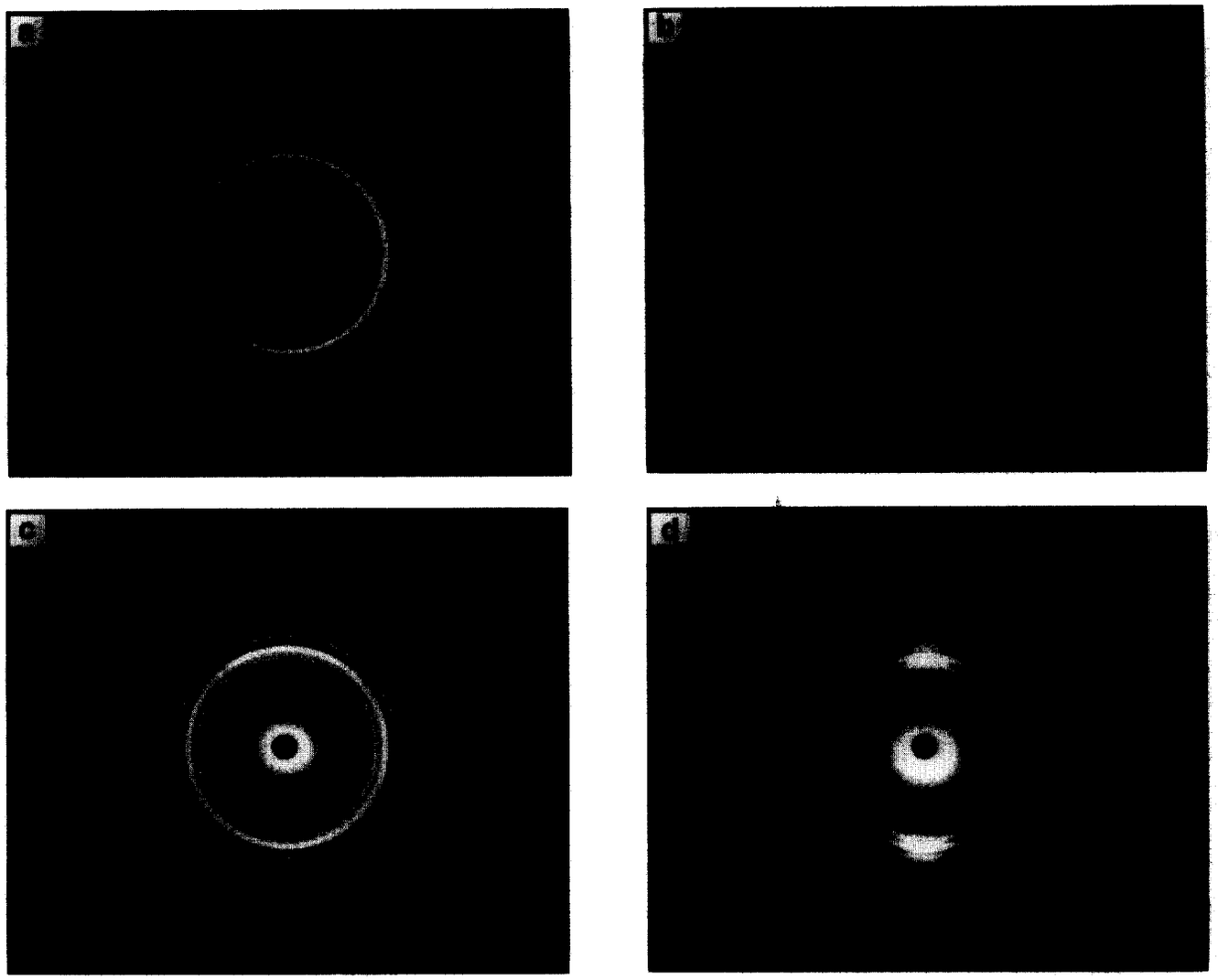

**Figure 5** Full image plate WAXS patterns for annealed C at various points on the load–extension curve. (a) Undeformed sample. (b) In the elastic region before yield. (c) Yield point, showing meridional monoclinic (0 0 1) reflection. (d) In the strain-softening region. (e) In the load–extension curve plateau at an extension of 25 mm. (f) From a sample taken to the yield point then relaxed without load for 1 h. (g) Simultaneously obtained load–extension curve. The tensile axis is vertical

(1 1 0) intensity was directly correlated with the increase in monoclinic ($\bar{2}$ 0 1) intensity. From *Figures 3*, *4* and *5* the appreciable increase in molecular orientation during strain-softening can be clearly seen. The orthorhombic (2 0 0) reflection oriented most rapidly, as shown in *Figures 3a* and *4a*. At the first yield point the orthorhombic (2 0 0) reflection oriented towards the equator, forming an arc then a two point pattern. The orthorhombic (0 2 0) followed the (2 0 0) reflection. In all samples the orthorhombic (1 1 0) reflection formed a weak four point pattern after the first yield point, as may be seen in frames 4 and 5 of *Figure 3*. The relation of the orthorhombic (1 1 0) reflection orientation to the load–extension curves is shown in *Figure 7* for the untreated and annealed LLDPE and MDPE samples. Where two yield points were apparent the four point pattern occurred at the second yield point. The four point pattern persisted during strain softening and into the plateau region of the load–extension curve, evolving into an arc centred on the equator.

For the untreated LLDPE samples the extension range over which the four point pattern persisted was roughly correlated with the percentage crystallinity; with the exception of untreated I the higher the percentage crystallinity the smaller the extension range over which the four point pattern existed. For the annealed LLDPE samples and the MDPE sample the four point pattern generally existed over a greater extension range in the more crystalline samples.

The virtual lack of change in intensity of the equatorial WAXS reflections, shown in *Figure 10*, from the region adjacent to the neck in annealed and untreated I and annealed H demonstrates the localization of deformation, regardless of branch type or thermal history. Virtually all of the deformation occurs in the neck.

*Relaxation of the monoclinic phase*

For samples C and H, which were allowed to relax without load after being taken to the yield point, all traces of the monoclinic phase disappeared. The WAXS patterns of the undeformed sample, yielded sample and relaxed sample clearly illustrate this in *Figures 5a*, *c* and *f* respectively. It can be seen that after relaxation the WAXS pattern had regained its initial isotropy.

*SAXS*

It was noted that the long spacing from SAXS was different to the long spacing from d.s.c. *Table 3* shows the

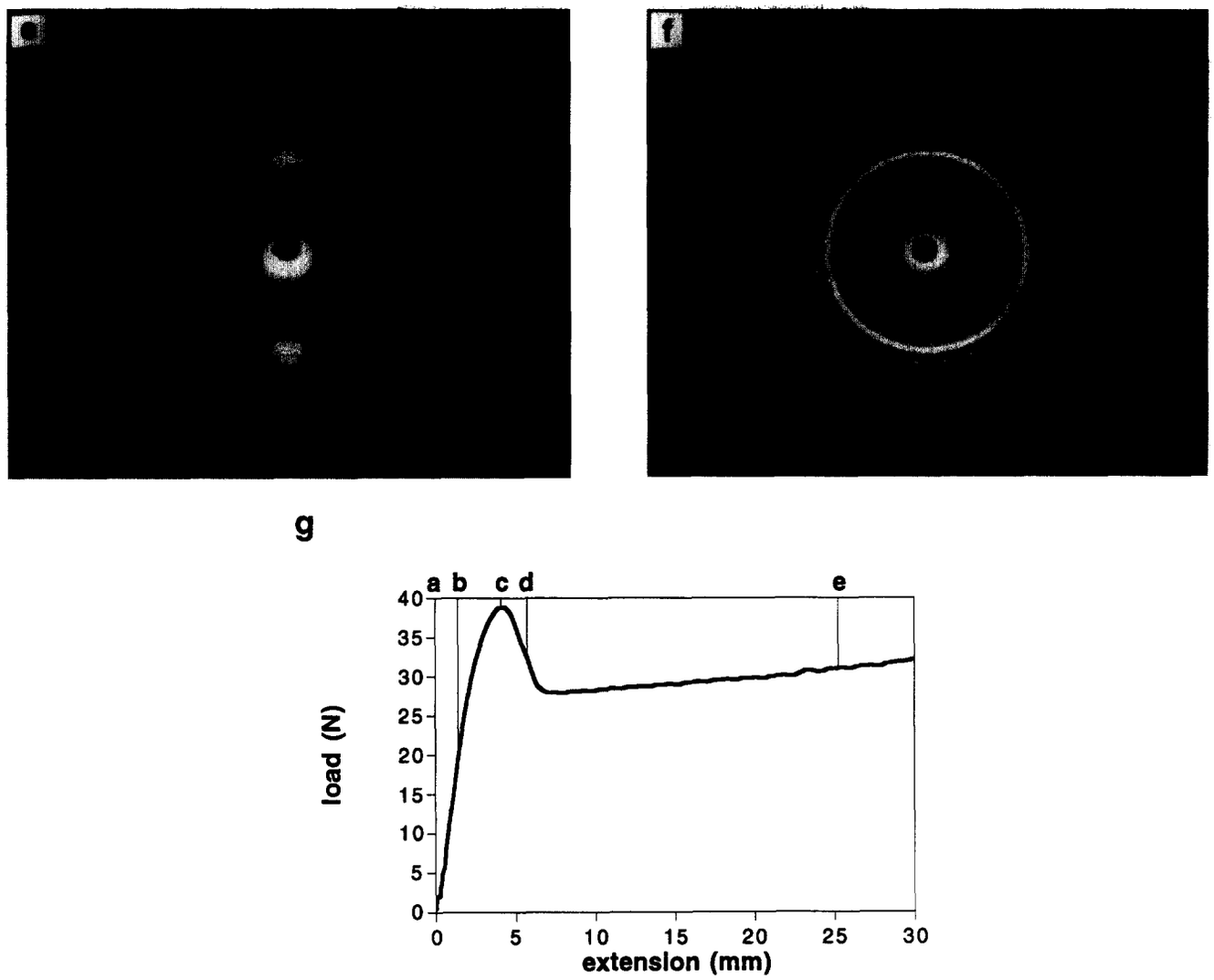


**Figure 5** Continued

long spacings measured by the two different methods. The ratio of SAXS to d.s.c. long spacing was found to be constant for samples with the same thermal history. The ratio was higher for the annealed LLDPE samples compared to their unannealed counterparts. Both unannealed and annealed MDPE had the same ratio, which was higher than for the LLDPE.

During deformation no voids were formed in any of the samples and lamellar scattering was measured over the whole deformation range. *Figure 3* shows a sequence of SAXS patterns with the simultaneously obtained load–extension curve. The equatorial and meridional long spacings are shown superimposed on the load–extension curve in *Figure 11* for samples C, G and J. In all samples the meridional long spacing increased whereas equatorially it decreased. For all samples, three regimes of behaviour were observed: an initial regime in which the long spacing remained unchanged, a second one in which the long spacings began to change and a final regime in which the changes continued but at a slower rate. These changes were related to the load–extension curve and to events measured by WAXS. The changes in long spacing began just before the (first) yield point and, with the exception of unannealed J, at the same extension at which the martensitic transformation was activated. This is shown in *Table 4*.

Equatorially, for both unannealed and annealed LLDPE samples, the long spacing for H showed the greatest percentage reduction, followed by G, then J and finally I. The MDPE grade C experienced a higher percentage decrease than the LLDPE grades. A plot of the percentage decrease against percentage crystallinity is shown in *Figure 12*, showing the relation between the percentage decrease and the amount of amorphous material. However, apart from the fact that the annealed samples all showed a faster rate of increase of meridional long spacing than their annealed counterparts, as shown in *Figure 13*, there was no evident correlation of the rate of increase of meridional long spacing with percentage crystallinity.

Shown in *Figure 11*, a new meridional long spacing appeared during strain hardening. Although very weak, it was detected in all samples. In most cases it appeared at the onset of the plateau region after strain softening ceased, although in untreated C, untreated and annealed I, and annealed J it was not identified with complete confidence until well within the plateau region. For annealed C all lamellar scattering disappeared during yielding and in unannealed C it disappeared just beyond the start of the load–extension curve plateau. For all samples, regardless of branch amount, type and distribution, thermal history, percentage crystallinity and initial

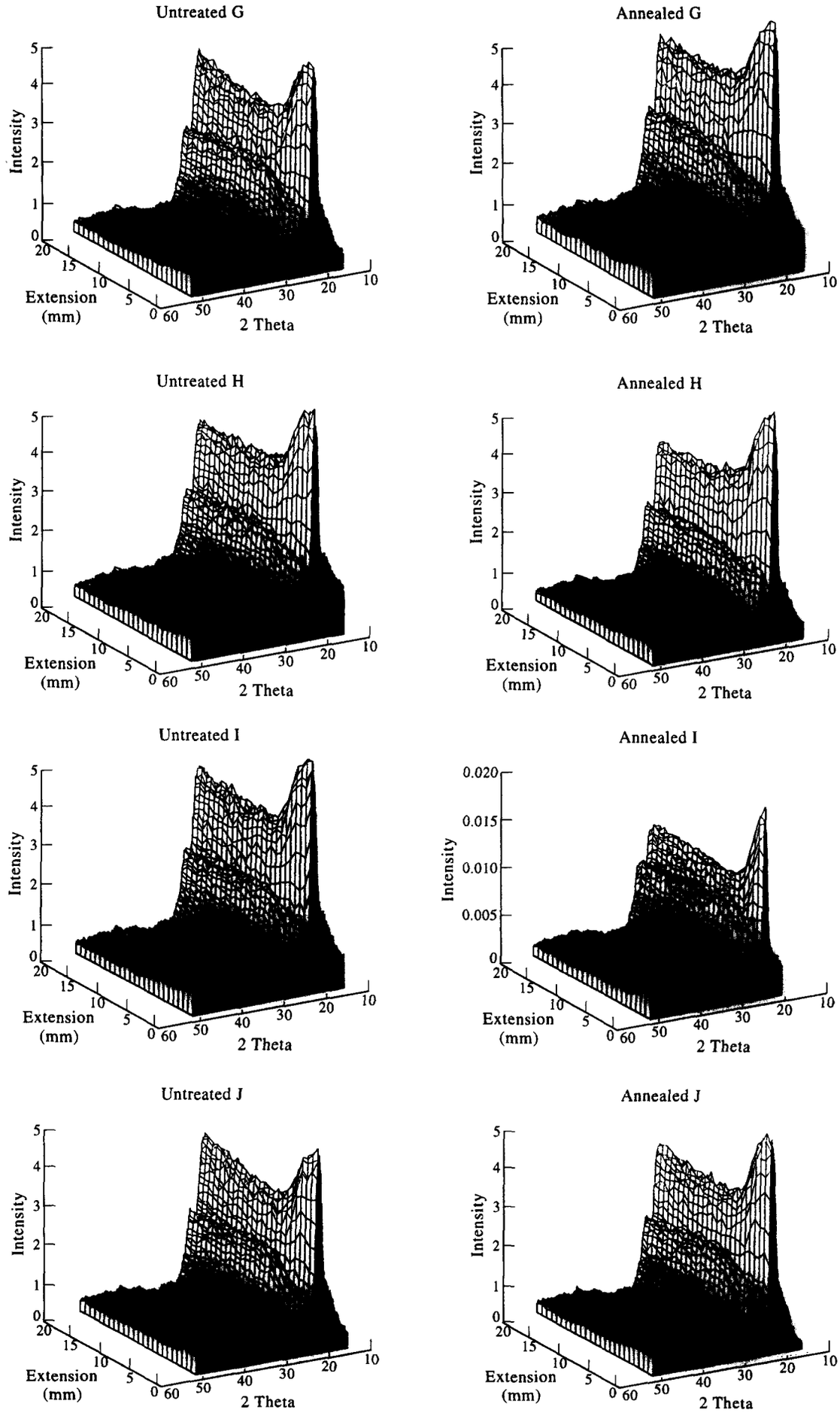


**Figure 6** Evolution of the WAXS intensities for untreated and annealed LLDPE samples, showing basic similarity in behaviour independent of thermal history, branch type and branch distribution

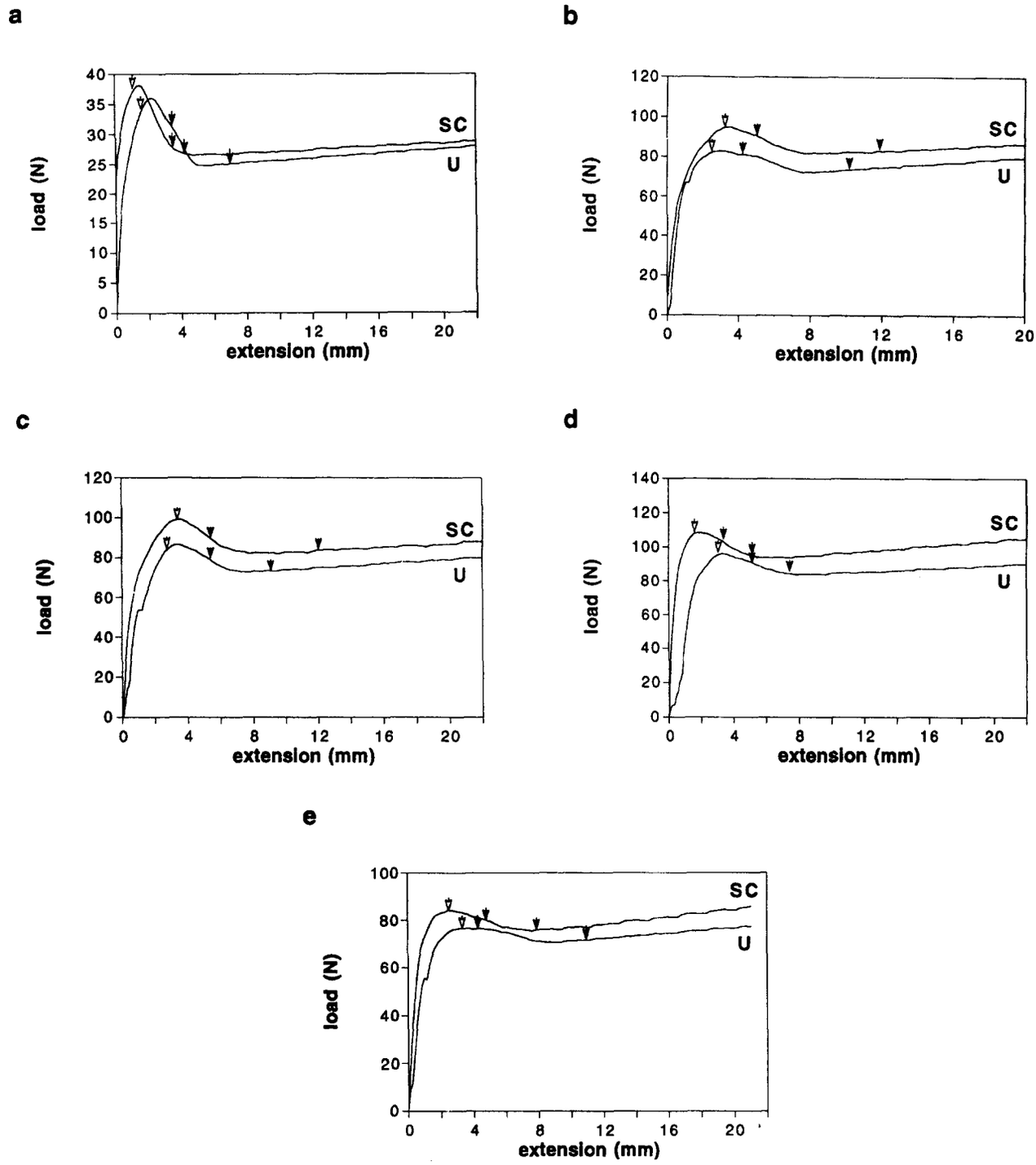


**Figure 7** Load–extension curves for all copolymer samples, showing the extension at which the martensitic transformation was activated (white arrow) and the extension range between which the orthorhombic (1 1 0) reflection was a four point pattern (marked by the black arrows). (a) C, (b) G, (c) H, (d) I, (e) J

lamellar thickness, the new meridional long spacing was the same, and was $11.5 \pm 0.4$ nm.

During drawing the meridional SAXS intensity distribution remained unaltered for all samples, decreasing in intensity but retaining the original profile. Equatorially the distribution changed, with more scattering detected at higher $q$ values. The increase in equatorial scattering at higher $q$ coincided with the onset of the changes in long spacings. The evolution of the SAXS intensities measured meridionally (parallel to LD) and equatorially (perpendicular to LD) are shown in *Figure 14* for the untreated LLDPE samples, showing the fundamental similarity regardless of branch type. *Figure 15* shows the evolution in the region adjacent to the neck for untreated and annealed I, demonstrating the lack of lamellar deformation in this region.

*Results for the linear HDPE*

The basic results for a linear HDPE, sample B, with comparable $M_w$ to the branched samples, are summarized here for comparison with the branched PE grades. More detailed behaviour of this sample has been described previously[15]. The major difference between the HDPE and the PE copolymers was the occurrence of voiding at the yield point, shown by a dramatic increase in SAXS intensity and characteristic equatorial

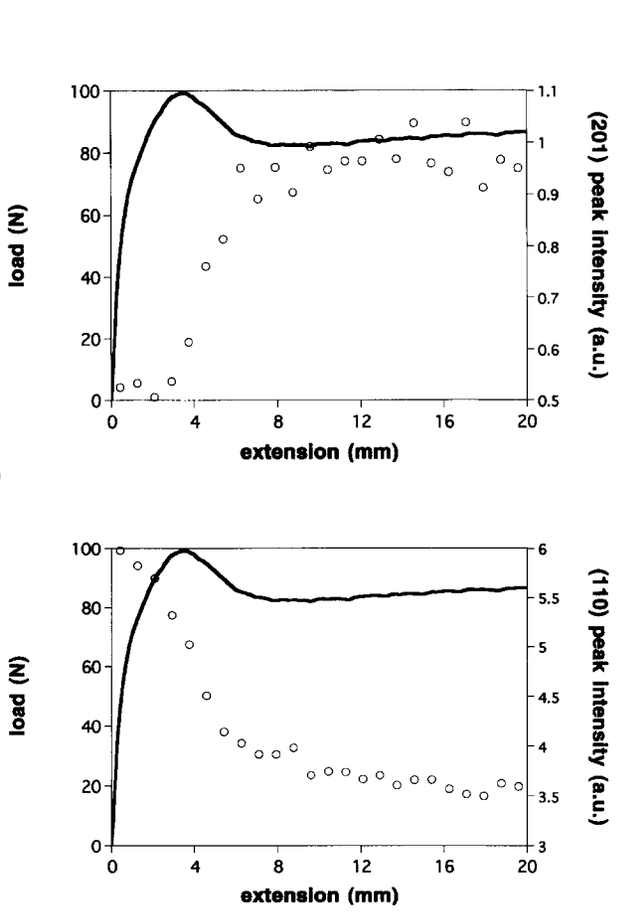


**Figure 8** Equatorial orthorhombic (1 1 0) intensities and load–extension curves for a variety of samples, showing the change during yield and strain softening and constant intensity during the load–extension plateau

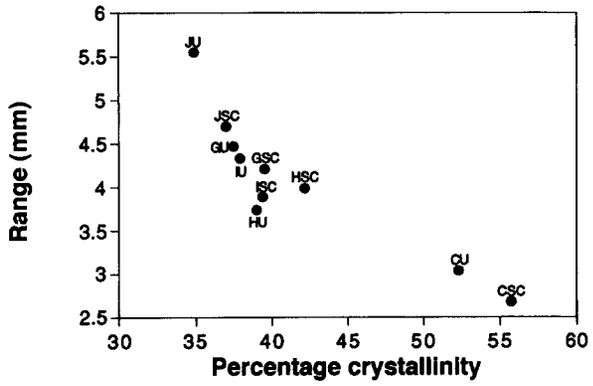


**Figure 9** Relation between the range over which the martensitic transformation was active, which was also a direct measure of the sharpness of the macroscopic yield, and the percentage crystallinity for the copolymer samples

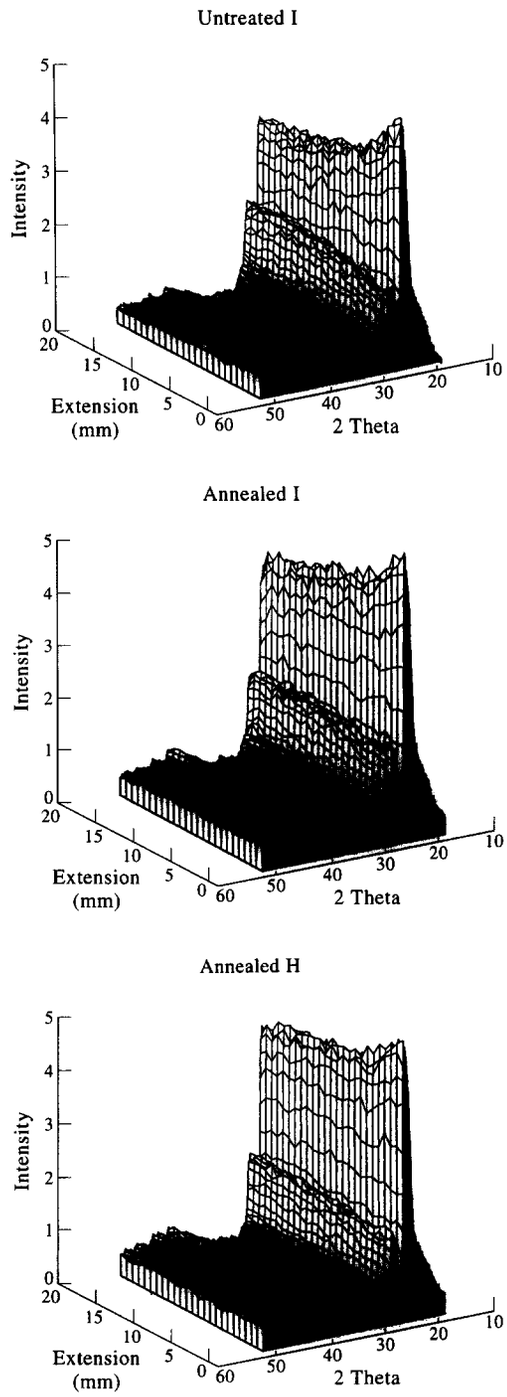


**Figure 10** Evolution of the WAXS intensities from the region adjacent to the neck in untreated and annealed I and annealed H

streaking. *Figure 16* shows the SAXS patterns from HDPE for comparison with the SAXS from the copolymers at a similar deformation.

Annealing caused lamellar thickening as well as an increase in percentage crystallinity. After drawing the percentage crystallinity decreased significantly, from $(74.9 \pm 0.3)\%$ to $(58.7 \pm 0.5)\%$. The correlations of the WAXS peak intensities and orientation behaviour were the same as for the MDPE and LLDPE. The extensions at which the martensitic transformation and molecular orientation began were lower than for the branched PE, and the rate of molecular orientation was more rapid. No four point pattern was observed for the orthorhombic (1 1 0) reflection. The onset of the martensitic transformation, shown by WAXS, and void formation, shown by SAXS, coincided with the yield point, shown in *Figure 15*. The yield point was sharper than for the branched samples. The evolution of the WAXS intensities for the HDPE sample compared to the LLDPE sample H can be seen in ref. 15, in which the more rapid changes in peak intensities for the HDPE are shown. Sample H was chosen since it has the most similar $M_w$ to the HDPE.

Both equatorial and meridional SAXS intensity distributions remained unchanged until the lamellar scattering became completely overwhelmed by void

**Table 3** SAXS and d.s.c. long spacings

| Sample | SAXS long spacing, $L_{SAXS}$ (nm) | D.s.c. long spacing, $L_{d.s.c.}$ (nm) | $L_{SAXS}/L_{d.s.c.}$ |
|---|---|---|---|
| B | 37.0 ± 1.0 | 51.5 ± 3.3 | 0.72 ± 0.05 |
| C U | 19.7 ± 1.1 | 26.5 ± 2.3 | 0.74 ± 0.08 |
| C SC | 24.1 ± 1.1 | 32.1 ± 2.8 | 0.75 ± 0.07 |
| G U | 17.8 ± 1·0 | 32.7 ± 2.8 | 0.54 ± 0.06 |
| G SC | 22.3 ± 1.0 | 33.7 ± 2.9 | 0.66 ± 0.06 |
| H U | 20.2 ± 1.0 | 36.8 ± 3.2 | 0.54 ± 0.05 |
| H SC | 24.6 ± 1.0 | 35.0 ± 3.0 | 0.70 ± 0.07 |
| I U | 19.2 ± 1.0 | 36.3 ± 3.1 | 0.53 ± 0.05 |
| I SC | 24.4 ± 1.6 | 36.0 ± 3.9 | 0.68 ± 0.08 |
| J U | 17.2 ± 1.0 | 35.5 ± 3.2 | 0.49 ± 0.05 |
| J SC | 22.1 ± 1.3 | 34.7 ± 3.0 | 0.64 ± 0.07 |

scattering, the onset of which coincided with the onset of the martensitic transformation. The rate of increase of the meridional long spacing was more rapid than for branched PE. The equatorial long spacing remained unchanged. No new meridional long spacing was observed.

## DISCUSSION

*D.s.c.*

Both annealing and drawing provided the means to order the potentially crystallizable material in untreated MDPE and LLDPE. The increase in percentage crystallinity during drawing for the untreated samples can be attributed to stress-induced crystallization due to straining of the amorphous component. The increase during annealing can be attributed to the growth of smaller lamellar crystals between those initially present. These are responsible for the extra melting endotherms in the annealed samples[24]. In LLDPE, with many branches, no lamellar thickening can occur on annealing whereas in MDPE fewer branches result in longer crystallizable units and lamellar thickening does occur. The linear molecules in HDPE allow lamellae to thicken appreciably[17].

That there is no increase in crystallinity for the drawn annealed LLDPE samples suggests that there is no more crystallizable material. Destruction of the thinner lamellae explains the almost total disappearance of the low temperature melting endotherms in the annealed LLDPE samples. It is expected that the newly formed interlamellar crystallites will be less perfect[24]. Thus, the smaller length of chain that is required to slip, and the fact that they are surrounded by a lot of amorphous material which will bear significant deformation makes them more easily disrupted. It has also been suggested that the smaller size of these crystals and their resultant lower thermodynamic stability reduces their melting point and during drawing they may disappear by partially melting[25].

In the HDPE B and the MDPE C the decrease in percentage crystallinity during drawing may be explained by stress-induced decrystallization, whereby the lamellae are disrupted during deformation[26]. The difference in behaviour between the HDPE and LLDPE may be explained by the relative contributions of the amorphous and crystalline components to the deformation. In HDPE, the larger amount of crystalline material results in more extensive deformation of the lamellae because, although the amorphous material also becomes strained, the deformation is transferred to the crystalline lamellae at lower strains. The lamellae bear more deformation than in LLDPE, and suffer more drastic re-organization. The evidence from SAXS, in which a fibre long spacing was observed for LLDPE but not for HDPE, also shows that crystalline disruption was more complete in the HDPE. It is also possible that the chains in the HDPE and MDPE are able to disentangle or disengage from the crystals more easily than in LLDPE. It has already been speculated whether the loss of constraint due to cavitation leads to local stress relaxation[15]. The consequent relaxation of the chains would prevent stress-induced crystallization[27]. Relaxation in LLDPE is prevented by the decreased chain mobility and disentanglement resistance resulting from the presence of a large number of branches[3,11,14]. The decrease in percentage crystallinity suggests that the melting endotherm that appeared after drawing in C was due to fragments from the original lamellae rather than stress-crystallized material.

The difference in long spacing measured by SAXS and d.s.c. was previously noted for HDPE and LLDPE[15], and was attributed to the value of the fold surface energy being inaccurate in equation (1). Fitting the value of fold surface energy to match SAXS and d.s.c. long spacings using the ratios given in *Table 3* gives a value of $(49 \pm 4) \times 10^{-7}$ J cm$^{-2}$ for the untreated LLDPE, $(62 \pm 6) \times 10^{-7}$ J cm$^{-2}$ for the annealed LLDPE and $(69 \pm 6) \times 10^{-7}$ J cm$^{-2}$ for both MDPE samples. The former value agrees well with a value of $(46 \pm 5) \times 10^{-7}$ J cm$^{-2}$ from isothermally crystallized bulk PE reported in the literature[28]. The higher value for the annealed samples indicates the greater crystalline perfection and better defined fold surface caused by annealing[29]. However, the uncertainty in the phase structure of melt-crystallized PE[30] (an interfacial phase between the lamellae and the amorphous component is thought to constitute between 6% and 11% of HDPE and 10% to 20% of LLDPE[31]) and the fact that there are lamellar crystals present that are not very well defined, at least in LLDPE, makes interpretation of surface energy parameters difficult[32].

An important caveat regarding the comparison of SAXS and d.s.c. derived lamellar thicknesses concerns the actual quantity measured by each technique. SAXS measures the long spacing of lamellae that are in stacks sufficiently large enough to cause coherent scattering, which are likely to be the thicker lamellae. The melting point measured by d.s.c. is also a measure of the thicker, more perfectly formed lamellae. Therefore neither method delivers an unbiased figure for the lamellar thickness, and corrections that account for the distribution of lamellar thicknesses ought to be considered for a full quantitative analysis. Since that is not in the remit of this investigation this matter will only be mentioned for completeness. The aim was to draw to the readers attention the perhaps surprising constancy of the ratio of SAXS to d.s.c. long spacing.

*Comments on double yield points and deformation mechanism*

Interlamellar deformation during elastic deformation was identified by the increase in meridional long spacing[33–36]. The decrease in equatorial long spacing that occurs at the first yield point and the concentration of SAXS intensity on the equator can be attributed to lamellar thinning caused by chain slip[37]. Chain slip

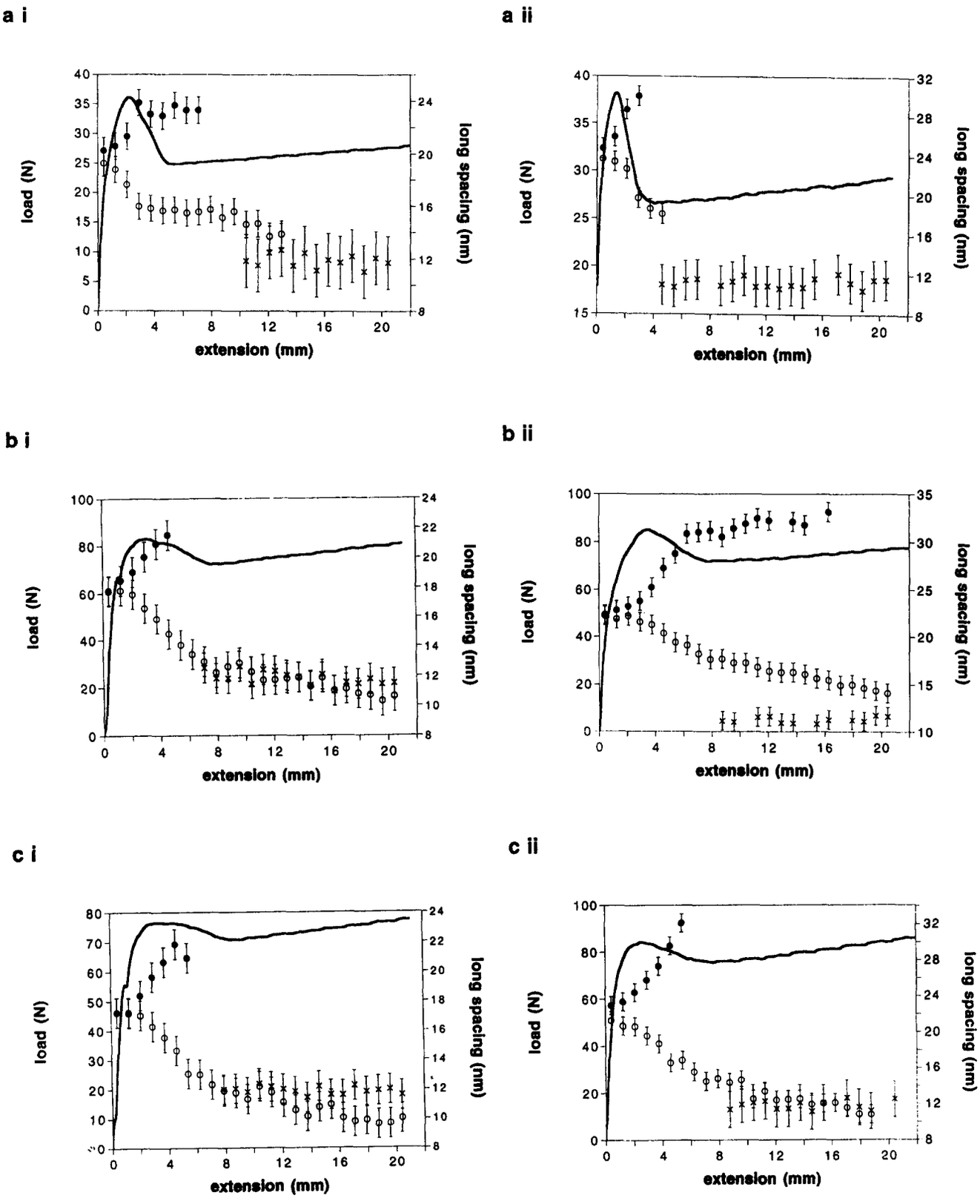


**Figure 11** Load–extension curves for (a) (i) and (a) (ii) untreated and annealed C respectively, (b) (i) and (b) (ii) untreated and annealed G respectively and (c) (i) and (c) (ii) untreated and annealed J respectively, with the load–extension curves superimposed. ● marks the long spacing measured meridionally, O is the equatorial long spacing and x is the fibre long spacing apparent after yielding

leading to lamellar rotation and thinning is schematically shown in frames 1 and 2 in *Figure 17*. The evidence for chain slip is supported firstly by the onset of the martensitic transformation at the first yield point. The occurrence of the martensitic transformation is to be regarded as an indication that plastic deformation is active. Chain slip is also a plastic deformation mechanism, with a slightly lower critical resolved shear stress than the martensitic transformation[38], and therefore it is expected that, for cold-drawn samples at least, chain slip and the martensitic transformation will coexist. Secondly, the rapid orientation of the orthorhombic (200) reflection,

**Table 4** Correlation of the extension at which the martensitic transformation became active, $e_{MT}$, detected by WAXS, with the extension at which lamellar orientation, $e_L$, was detected by SAXS

| Sample | $e_{MT}$ [mm (±0.42 mm)] | $e_L$ [mm (±0.42 mm)] |
|---|---|---|
| C U | 1.67 | 1.67 |
| C SC | 1.67 | 1.67 |
| G U | 2.50 | 2.50 |
| G SC | 3.33 | 3.33 |
| H U | 2.50 | 3.33 |
| H SC | 3.33 | 2.50 |
| I U | 3.33 | 3.33 |
| I SC | 1.67 | 1.67 |
| J U | 3.33 | 1.67 |
| J SC | 3.33 | 1.67 |

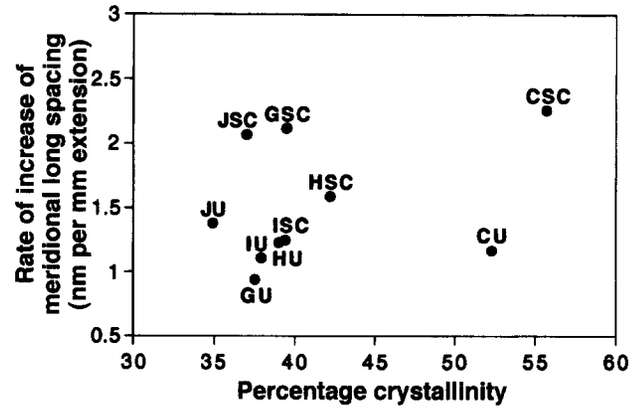


**Figure 12** Relation of the rate of increase of meridional long spacing with percentage crystallinity

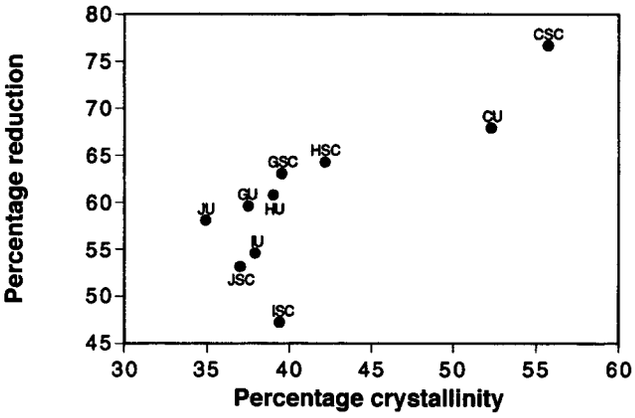


**Figure 13** Relation of the percentage decrease in equatorial long spacing with percentage crystallinity

that we have shown to begin at the first yield point, has been proposed to be due to (1 1 0) twinning followed by (1 0 0)[0 0 1] chain slip[39,40]. Although we cannot identify deformation twinning, the occurrence of chain slip is supported by, and supports, the other evidence. The process of chain slip which causes lamellar rotation and thinning may be identified with the fine chain slip model proposed by Bowden and Young[41]. The relaxation of lamellar orientation and martensitic transformation from the first yield point after unloading suggests reversible lamellar deformation up to this point, i.e. that the lamellae are intact at the first yield point.

The second yield point marks the onset of lamellar fragmentation, and the irreversible lamellar to fibrillar transformation described by Peterlin[42], whereby the original lamellae disintegrate and their remnants are incorporated into fibres. This is evident by the disappearance of the meridional lamellar long spacing at the second yield point and appearance of the meridional fibre long spacing after it, in *Figures 11b* and *c*. The disappearance of the meridional long spacing in the vicinity of the second yield point suggests that irreversible lamellar fragmentation occurred. In terms of mechanical deformation, Bowden and Young's coarse chain slip model[41], shown schematically going from frames 2 to 3 in *Figure 17*, provides a suitable mechanism for lamellar disintegration, resulting in the fibrillar texture in frame 4 of *Figure 17*. Chain slip on the ($h\,k$ 0)[0 0 1] slip systems ($c$ axis slip) is generally reckoned to be the means by which the overall oriented texture is finally achieved at higher extensions[40], and coarse slip has been found to be more important with increasing strain[43]. A more detailed study of double yield behaviour was made by Brooks *et al.*[44,45], who identified double yielding in B, C and G in various conditions. They suggested that at the second yield point the lamellae are tilted at the optimum angle for lamellar disintegration. Our finding that the orthorhombic (1 1 0) reflection, which is associated with tilted lamellae[45,46], forms a four point pattern near the second yield point supports this. Probably, the strain at which a particular lamella reaches the optimum orientation for lamellar disintegration depends on its initial orientation. There will therefore be a range of strains over which the preferred orientation is reached, which explains the observed coexistence of the lamellar and fibrillar morphologies.

Previously, the first yield has been proposed to result from lamellar re-orientation, with little disruption, and the second to be due to intra-lamellar shear resulting in lamellar fragmentation[44-49]. The percentage crystallinity influences the relative ease of these processes[49]. Lamellar fragmentation is favoured by the more regularly chain folded systems with well defined slip planes whereas the deeply intertwined folds which bridge all kinds of ($h\,k$ 0) planes in the less crystalline samples promote homogeneous shear. The results from the LLDPEs appear to confirm this argument since percentage crystallinity was apparently the main factor that determined whether two yield points were seen—two yield points were observed in the two least crystalline samples (untreated G and J) but were not present in their more crystalline annealed counterparts. Such an argument does not, however, explain why an apparent second yield point (albeit weak) was observed in the more crystalline MDPE sample, untreated C. Inspection of *Table 2*, however, shows that untreated C has thinner lamellae, even though it is more crystalline, than the LLDPE samples H and I, which only had one yield point. It is proposed that chain slip occurs more easily in the thinner lamellae, by virtue of the smaller length of chain that has to slide through the lamellae, which would encourage the fine chain slip mechanism (this argument also explains the preferential destruction of the thinner subsidiary lamellae in the annealed samples). Therefore, both lamellar thickness and percentage crystallinity contribute to the occurrence of double yielding.

Although the observations have been reasonably explained in terms of a purely mechanical deformation, for completeness an alternative mechanism, in terms of melting and recrystallization, must also be mentioned.

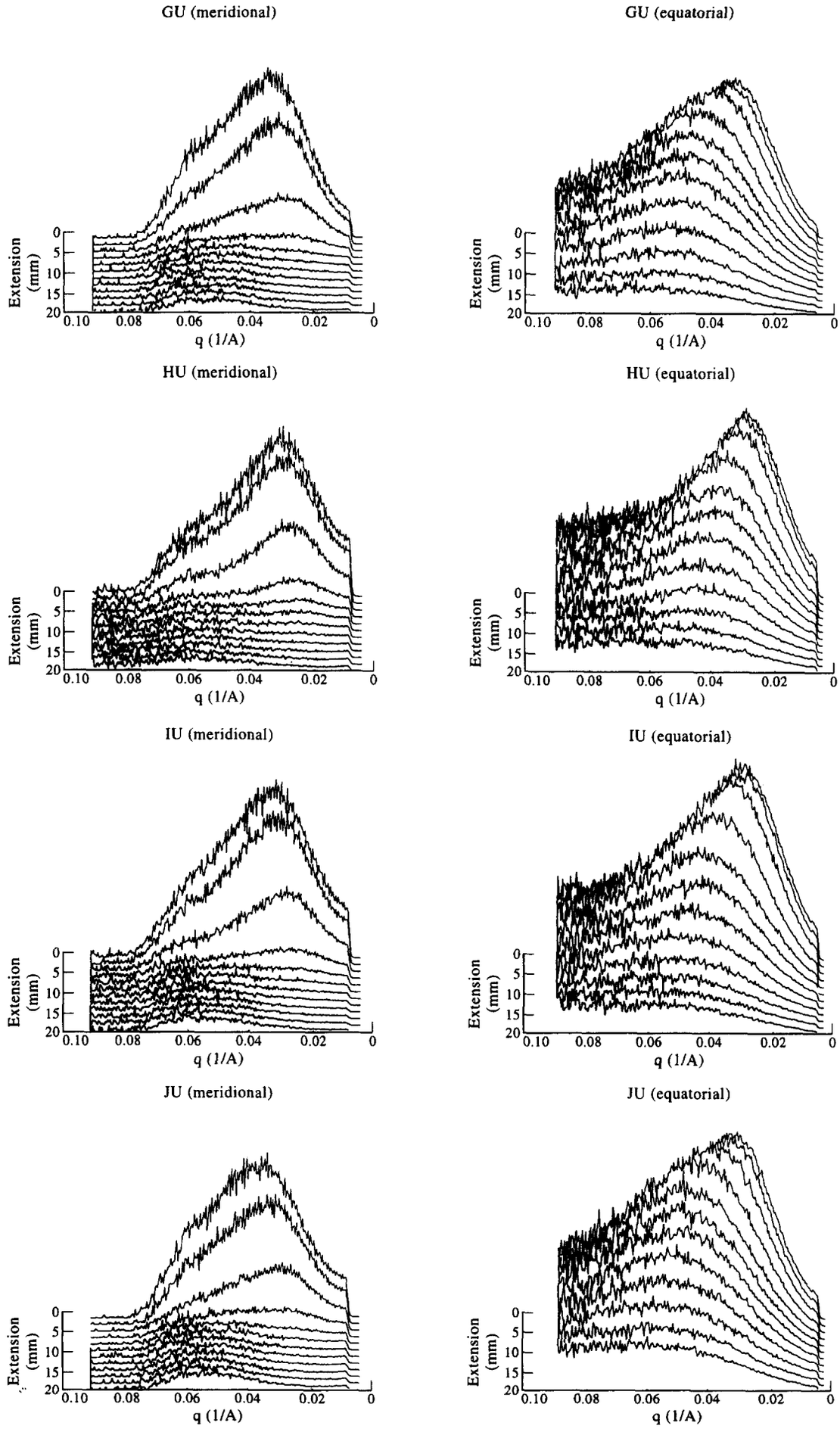


**Figure 14** *Evolution of the (Lorentz corrected) SAXS intensities for the untreated LLDPEs, demonstrating the fundamental similarity between them all*

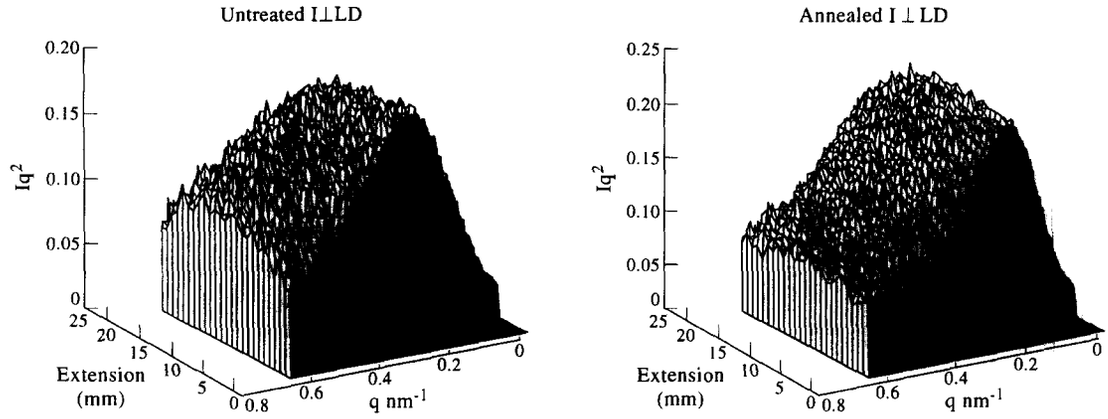


**Figure 15** Evolution of the equatorial (Lorentz corrected) SAXS intensity for untreated and annealed I measured in the region adjacent to the neck, showing the localization of the deformation on the lamellar length scale also

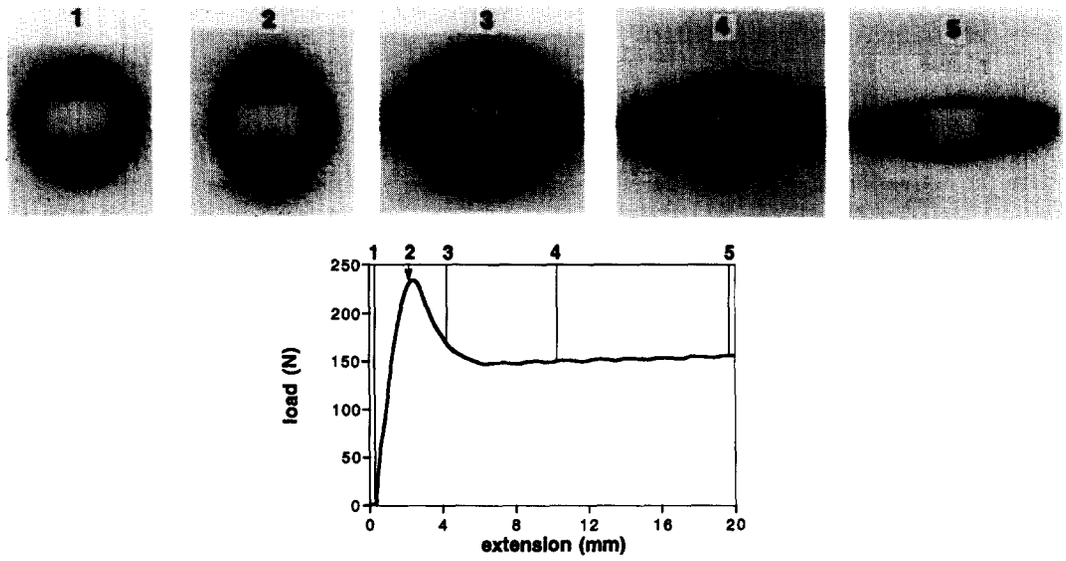


**Figure 16** Series of SAXS patterns with simultaneously obtained load–extension curve, from deformed HDPE, showing equatorial void scattering. Contrast these with the SAXS pattern from LLDPE, in *Figure 3*. The arrow on the load–extension curve marks the extension at which the martensitic transformation was activated. The WAXS patterns (not shown) were similar to those for LLDPE in *Figures 3* and *4*

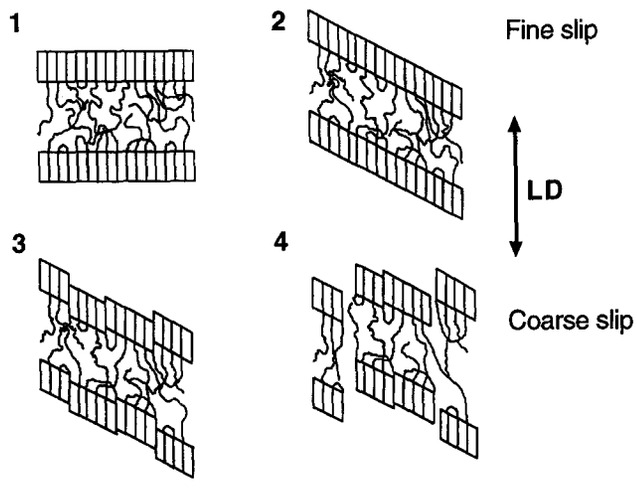


**Figure 17** Schematic representation of fine chain slip in lamellae followed by coarse chain slip leading to lamellar disintegration and fibre formation. The direction LD indicates the tensile axis

This mechanism also explains the observed dependence of double yielding on percentage crystallinity. A systematic study of double yield points in PE[25], in which the second yield point was enhanced as percentage crystallinity decreased, demonstrated the correlation of double yielding with decreasing percentage crystallinity for a range of PE co- and homo-polymers. It was proposed that during deformation the concentration of stress on the less perfect crystallites causes them to partially melt and recrystallize. Potentially crystallizable material formed a new population of oriented crystallites[25]. The two yield points therefore resulted from the yielding of the original and new crystallites separately. The less stable smaller crystals in the less crystalline samples melted and recrystallized more easily, enhancing the second yield point. Therefore the explanation that the thinner lamellae in untreated C are more susceptible to melting and recrystallization than those in the less crystalline LLDPE samples H and I lends itself. Melting of the subsidiary lamellae that form on annealing may

also explain the observation of only one lamellar thickness in the drawn annealed samples but three in the undeformed ones. Melting and recrystallization has been inferred from neutron scattering experiments[50,51], and is supported by the constant fibre long spacing, which was the same for all of the samples regardless of their initially different morphologies.

However, evidence against melting and recrystallization is provided by the continuous decrease in equatorial long spacing during deformation, since melting is expected to cause an increase in long spacing[52]. It is also unlikely that the heat of deformation would raise the sample temperature by a sufficient amount to melt the lamellae (a rise of approximately 100°C is required to melt the dominant lamellae in untreated G and J). Therefore, although melting and recrystallization cannot be completely discounted, it appears that the first yield point was due to fine chain slip and the second due to coarse slip resulting in lamellar fragmentation.

*The influence of branch amount*

In LLDPE, with its greater number of branches and consequently lower crystallinity, the amorphous component plays a larger role during deformation than in MDPE and HDPE. This is why the yield extension is higher and the yield point more diffuse as the branch content increases[1]. The increased amount of amorphous material results in the activation of crystalline deformation mechanisms at higher extensions[15], explaining the onset of the martensitic transformation and molecular orientation at progressively higher extensions as the amount of branches is increased from HDPE through MDPE to LLDPE. As well as there being more of it in LLDPE and HDPE, it is possible that the increased amount of amorphous deformation is also related to the ease of deformation of the crystals. It is possible that the crystals deform more easily in the HDPE. A linear chain is more mobile than a branched chain[3,11,14], and if deformation is to proceed chains must disentangle in the amorphous regions and be drawn through the crystals. The branches are expected to impede disentanglement, thus reducing the amount of chain slip.

The absence of a meridional fibre long spacing in HDPE may be explained by the greater lamellar disruption in HDPE. The voids that are formed in HDPE result in the final fibrillar structure containing less coherent scattering entities.

*The influence of branch type*

Although the samples with different branches behaved differently, the differences can be explained in terms of percentage crystallinity. Previous workers have stated that the branch type only affects the strain-hardening region of the load–extension curve in model ethylene-α-olefin copolymers[2] and that yield and small-deformation behaviour in both model copolymers and commercial materials is only affected by percentage crystallinity (a function of branch concentration and distribution and molecular weight)[53].

Both I and J contain approximately the same amount of butyl branches, but J is less crystalline. A greater amount of inter-lamellar relative to intra-lamellar deformation in J, resulting from the larger amount of interlamellar material, causes the activation of crystalline deformation mechanisms (indicated by the presence of the monoclinic phase and the decrease in equatorial long spacing) at higher extensions. J also has a lower long spacing than I and therefore a greater tie molecule density. A greater amount of deformation must be borne by the larger number of tie molecules before intra-lamellar deformation is activated. The yield extension is higher, molecular orientation less rapid, and the yield point more diffuse, leading to a higher extension at which the lamellar to fibrillar transformation occurs.

The greater importance of intra-lamellar deformation at lower strains in untreated I compared to G, which has the same percentage crystallinity but a different branch type, may be explained by the greater tie molecule density in G (G has a smaller long spacing and a higher $M_w$), using the same argument as for untreated J.

The thinner subsidiary lamellae that form in between the original dominant lamellae during annealing in the annealed samples may be expected to provide increased resistance to inter-lamellar deformation if they must be destroyed before sufficient inter-lamellar deformation can occur to activate deformation of the dominant lamellae. Crystallographic deformation mechanisms have a higher activation strain than mechanisms involving the amorphous component[34]. That the annealed samples with the highest percentage crystallinities (G and H), and therefore most inter-lamellar crystallites, show less rapid molecular orientation supports this argument, although the absence of the effect in sample I, which possessed a similar percentage crystallinity to G in both untreated and annealed samples is difficult to explain using this rationale. However, although they have similar percentage crystallinities they do not necessarily have the same morphology, witnessed by the difference in long spacings. Therefore it is possible that the branch amount and distribution, about which limited information is available for these samples, plays a significant role in the determination of the details of the deformation mechanisms. Further investigation with a set of well characterized samples is clearly necessary to resolve these problems.

The differences in martensitic transformation strain in the annealed samples compared to unannealed ones may also result from the effect of crystalline perfection. A higher martensitic transformation strain, as found in annealed G and H compared to their unannealed counterparts, was previously explained by the greater crystallinity of the annealed sample promoting the ease and/or amount of chain slip at the expense of the martensitic transformation[15]. The effect is less pronounced in J, for which the annealed sample has a lower percentage crystallinity than G and H. There is no clear explanation for the reverse trend observed for I. That it may be related to percentage crystallinity is again suggested, however, by the fact that of the annealed samples I has the lowest percentage crystallinity.

The different rates of lamellar separation during elastic deformation cannot readily be explained in terms of branch length, since there is no apparent trend with increasing branch length. It is expected that the bulky iso-butyl branches in H would inhibit deformation more than the smaller and more flexible ethyl and butyl branches in C, G, I and J. However, for a given sample, in the annealed samples interlamellar separation occurred more readily than in the unannealed samples. Comparison of the HDPE used in this study, and other HDPE samples[54], showed a more rapid rate of lamellar separation in these more crystalline systems. The reduced

amount of amorphous material, with fewer entanglements per chain, that results from annealing and increasing crystallinity and crystalline perfection, probably resists deformation less. Possibly the difference between annealed and unannealed samples reflects an ordering of the interfacial component, known to be where most of the branches reside[55], upon annealing, which affects the ease of lamellar separation. The interfacial component may be similar for all of the unannealed samples, explaining why the rate of increase of meridional long spacing is approximately the same for all of the unannealed samples. The percentage reduction in equatorial long spacing is directly related to the amount of amorphous material. A greater percentage crystallinity allows a greater amount of lamellar deformation. An increased amount of lamellar thinning due to chain slip could account for the larger decrease in equatorial long spacing for the more crystalline samples in which crystallographic deformation is more prominent.

## CONCLUSIONS

The results show that for commercial grade polyethylenes percentage crystallinity is of great importance in determining the tensile deformation behaviour. It does this by influencing the relative importance of deformation modes involving the crystalline and non-crystalline components respectively.

By increasing the number of branches the percentage crystallinity and long spacing are reduced, and the tie molecule density increased. The relative importance of the non-crystalline component is increased and crystalline deformation mechanisms are activated at higher extensions. Hence the yield point becomes more diffuse as branching increases.

The chemical species of side chain branch has a negligible effect upon the tensile deformation behaviour for the deformation range studied. The branch distribution is of greater importance via its influence on percentage crystallinity, long spacing and therefore tie molecule density. It has also been shown that the lamellar population affects the deformation behaviour; interlamellar crystallites formed on annealing impede deformation of the amorphous component.

In systems exhibiting a double yield, the first yield is totally reversible and apparently corresponds to the onset of fine chain slip. The second yield is irreversible and seems to correspond to lamellar fragmentation via coarse chain slip. A stress-induced martensitic transformation coexists with chain slip, and indicates that yielding and strain softening is associated with crystallographic deformation mechanisms.

## ACKNOWLEDGEMENTS

The help of the following people is gratefully acknowledged: Dr Elinor Kerr, of BP Chemicals, Mary Vickers, of the Department of Materials Science and Metallurgy, University of Cambridge, Pete Bone and Lara Stoimenof, of the Cavendish Laboratory, University of Cambridge, and Mary Heppenstall-Butler, of UMIST. We are indebted to staff at the CCLRC Daresbury Laboratory, including Elizabeth Towns-Andrews, Geoff Mant and Anthony Gleeson, for their technical support which enabled these experiments to be performed and for the provision of programs from the CCP13 software suite which were employed in the data analysis. The financial support of the EPSRC and BP Chemicals is acknowledged.

## REFERENCES

1. Capaccio, G. and Ward, I. M., *J. Polym. Sci., Polym. Phys. Edn*, 1984, **22**, 475.
2. Kennedy, M. A., Peacock, A. J., Failla, M. D., Lucas, J. C. and Mandelkern, L., *Macromolecules*, 1995, **28**, 1407.
3. Lu, X., Wang, X. and Brown, N., *J. Mater. Sci.*, 1988, **23**, 643.
4. Huang, Y.-L. and Brown, N., *J. Polym. Sci., Polym. Phys. Edn*, 1991, **29**, 129.
5. Lustiger, A. and Markham, R. L., *Polymer*, 1983, **24**, 1647.
6. Bubeck, R. A. and Baker, H. M., *Polymer*, 1982, **23**, 1680.
7. Alamo, R. G., Viers, B. D. and Mandelkern, L., *Macromolecules*, 1993, **26**, 5740.
8. France, C., Hendra, P. J., Maddams, W. F. and Willis, H. A., *Polymer*, 1987, **28**, 710.
9. Hay, J. N. and Zhou, X.-Q., *Polymer*, 1993, **34**, 1002.
10. Brown, N. and Ward, I. M., *J. Mater. Sci.*, 1983, **18**, 1405.
11. Zhou, Z. and Brown, N., *Polymer*, 1994, **35**, 3619.
12. Zhou, Z., Lu, X. and Brown, N., *Polymer*, 1993, **34**, 2520.
13. Brown, N. and Zhou, Z., *Macromolecules*, 1995, **28**, 1807.
14. de Gennes, P. G., in *Scaling Concepts in Polymer Physics*. Cornell University, New York, 1979.
15. Butler, M. F., Donald, A. M., Bras, W., Mant, G. R., Derbyshire, G. E. and Ryan, A. J., *Macromolecules*, 1995, **28**, 6383.
16. Hoffman, J. D., Davis, G. T. and Lauritzen, J. I. Jr., in *Treatise on Solid State Chemistry*, Vol. 3. Plenum Press, New York, 1976.
17. Wunderlich, B., in *Macromolecular Physics*, Vol. 1. Academic Press, New York, 1973.
18. Towns-Andrews, E., Berry, A., Bordas, J., Mant, G. R., Murray, P. K., Roberts, K., Sumner, I., Worgan, J. S., Lewis, R. A. and Gabriel, A., *Rev. Sci. Instr.*, 1989, **60**, 2346.
19. Bliss, N., Bordas, J., Fell, B. D., Harris, N. W., Helsby, W. I., Mant, G. R., Smith, W. and Towns-Andrews, E., *Rev. Sci. Instr.*, 1995, **66**, 1311.
20. Bilsborrow, R. L., Bliss, N., Bordas, J., Cernik, R. J., Clark, G. F., Clark, S. M., Collins, S. P., Dobson, B. R., Fell, B. D., Grant, A. F., Harris, N. W., Helsby, W. I., Smith, W. and Towns-Andrews, E., *Rev. Sci. Instr.*, 1995, **66**, 1633.
21. Bras, W., Mant, G. R., Derbyshire, G. E., O'Kane, W. J., Helsby, W. I., Hall, C. J. and Ryan, A. J., *J. Synchr. Rad.*, 1995, **2**, 87.
22. Lee, Y. D., Phillips, P. J. and Lin, J. S., *J. Polym. Sci., Polym. Phys. Edn.*, 1991, **29**, 1235.
23. Baltà-Calleja, F. J. and Vonk, C., in *X-ray Scattering of Polymers*. Elsevier, Amsterdam, 1989.
24. Bassett, D. C., in *Principles of Polymer Morphology*. Cambridge University Press, New York, 1981.
25. Lucas, J. C., Failla, M. D., Smith, F. L. and Mandelkern, L., *Polymer Eng. Sci.*, 1995, **35**, 1117.
26. Brady, J. M. and Thomas, E. L., *J. Mater. Sci.*, 1989, **24**, 3311.
27. Brady, J. M. and Thomas, E. L., *J. Mater. Sci.*, 1989, **24**, 3319.
28. Varnell, W. D., Harrison, I. R., Wang, J. I., *J. Polym. Sci., Polym. Phys. Edn.*, 1981, **19**, 1577.
29. Wunderlich, B., in *Macromolecular Physics*, Vol. 2. Academic Press, New York, 1973.
30. Naylor, C. C., Meier, R. J., Kip, B. J., Williams, K. P. J., Mason, S.-M., Conroy, N. and Gerrard, D. L., *Macromolecules*, 1995, **28**, 2969.
31. McFaddin, D. C., Russell, K. E., Gang, W. and Heyding, R. D., *J. Polym. Sci., Polym. Phys. Edn.*, 1993, **31**, 175.
32. Wunderlich, B., in *Macromolecular Physics*, Vol. 3. Academic Press, New York, 1973.
33. Pope, D. P. and Keller, A., *J. Polym. Sci., Polym. Phys. Ed.*, 1975, **13**, 533.
34. Pope, D. P. and Keller, A., *J. Mater. Sci.*, 1971, **6**, 453.
35. Bartczak, Z., Cohen, R. E., Argon, A. S., *Macromolecules*, 1992, **25**, 4692.
36. Peterlin, A. and Meinel, G., *Makromol. Chem.*, 1971, **142**, 227.
37. Cowking, A. and Rider, J. G., *J. Mater. Sci.*, 1969, **4**, 1051.
38. Lin, L. and Argon, A. S., *J. Mater. Sci.*, 1994, **29**, 294.
39. Meinel, G., Morosoff, N. and Peterlin, A., *J. Polym. Sci. A-2*, 1970, **8**, 1723.
40. Krause, S. J. and Hosford, W. F., *J. Polym. Sci., Polym. Phys. Edn.*, 1989, **27**, 1853.

41. Bowden, P. B. and Young, R. J., *J. Mater. Sci.*, 1974, **9**, 2034.
42. Peterlin, A., *J. Mater. Sci.*, 1971, **6**, 490.
43. Burnay, S. G., Aere, M. D. D. and Groves, G. W., *J. Mater. Sci.*, 1978, **13**, 639.
44. Brooks, N. W., Duckett, R. A. and Ward, I. M., *Polymer*, 1992, **33**, 1872.
45. Brooks, N. W. J., Unwin, A. P., Duckett, R. A. and Ward, I. M., *J. Macromol. Sci.–Phys.*, 1995, **B34**, 29.
46. Vickers, M. E. and Fischer, H., *Polymer*, 1995, **36**, 2667.
47. Balsamo, V. and Müller, A. J., *J. Mater. Sci. Lett.*, 1993, **12**, 1457.
48. Séguéla, R. and Rietsch, F., *J. Mater. Sci. Lett.*, 1990, **9**, 46.
49. Séguéla, R. and Darras, O., *J. Mater. Sci.*, 1994, **29**, 5342.
50. Wignall, G. D. and Wu, W., *Polym. Commun.*, 1983, **24**, 354.
51. Wu, W., Wignall, G. D. and Mandelkern, L., *Polymer*, 1983, **33**, 4137.
52. Ryan, A. J., Bras, W., Mant, G. R. and Derbyshire, G. E., *Polymer*, 1994, **35**, 4357.
53. Fatou, J. G., Maciá, I. G., Marco, C., Gómez, M. A., Arribas, J. M., Fontecha, A., Aroca, M. and Martínez, M. C., *J. Mater. Sci.*, 1996, **31**, 3095.
54. Butler, M., Donald, A. M. and Ryan, A. J., *Polymer*, (in press)
55. Alamo, R. G., Viers, B. D. and Mandelkern, L., *Macromolecules*, 1993, **26**, 5740.